J Biomol NMR (2015) 61:137–150
DOI 10.1007/s10858-014-9895-2

ARTICLE

Comparison of backbone dynamics of the type III antifreeze protein and antifreeze-like domain of human sialic acid synthase

Yong-Geun Choi · Chin-Ju Park · Hee-Eun Kim · Yeo-Jin Seo · Ae-Ree Lee · Seo-Ree Choi · Shim Sung Lee · Joon-Hwa Lee

Received: 2 November 2014 / Accepted: 30 December 2014 / Published online: 10 January 2015

Abstract Antifreeze proteins (AFPs) are found in a variety of cold-adapted (psychrophilic) organisms to promote survival at subzero temperatures by binding to ice crystals and decreasing the freezing temperature of body fluids. The type III AFPs are small globular proteins that consist of one α-helix, three 3_{10}-helices, and two β-strands. Sialic acids play important roles in a variety of biological functions, such as development, recognition, and cell adhesion and are synthesized by conserved enzymatic pathways that include sialic acid synthase (SAS). SAS consists of an N-terminal catalytic domain and a C-terminal antifreeze-like (AFL) domain, which is similar to the type III AFPs. Despite having very similar structures, AFL and the type III AFPs exhibit very different temperature-dependent stability and activity. In this study, we have performed backbone dynamics analyses of a type III AFP (HPLC12 isoform) and the AFL domain of human SAS (hAFL) at various temperatures. We also characterized the structural/dynamic properties of the ice-binding surfaces by analyzing the temperature gradient of the amide proton chemical shift and its correlation with chemical shift deviation from random coil. The dynamic properties of the two proteins were very different from each other. While HPLC12 was mostly rigid with a few residues exhibiting slow motions, hAFL showed fast internal motions at low temperature. Our results provide insight into the molecular basis of thermostability and structural flexibility in homologous psychrophilic HPLC12 and mesophilic hAFL proteins.

Keywords NMR · Backbone dynamics · Antifreeze protein · Antifreeze-like protein · Ice-binding protein

Abbreviations

AFP	Antifreeze protein
QAE	Quaternary-amino-ethyl
SP	Sulfopropyl
TH	Thermal hysteresis
IBS	Ice-binding surface
AFL	Domain antifreeze-like domain
Sialic acid	*N*-acetylneuraminic acid
SAS	Sialic acid synthase
PEP	Phosphoenolpyruvate
ManNAc	*N*-acetylmannosamine
NeuNAc	*N*-acetylneuraminic acid
ManNAc-6P	ManNAc 6-phosphate
NeuNAc-9P	NeuNAc 9-phosphate
3D	Three-dimensional
CSD	Chemical shift deviation
H-bond	Hydrogen-bond
NOE	Nuclear Overhauser effect

Yong-Geun Choi and Chin-Ju Park have contributed equally to this work.

Electronic supplementary material The online version of this article (doi:10.1007/s10858-014-9895-2) contains supplementary material, which is available to authorized users.

Y.-G. Choi · H.-E. Kim · Y.-J. Seo · A.-R. Lee · S.-R. Choi · S. S. Lee · J.-H. Lee (✉)
Department of Chemistry and Research Institute of Natural Science, Gyeongsang National University, Jinju, Gyeongnam 660-701, Republic of Korea
e-mail: joonhwa@gnu.ac.kr

C.-J. Park
Division of Liberal Arts and Sciences and Department of Chemistry, Gwangju Institute of Science and Technology, Gwangju 500-712, Republic of Korea

Introduction

Antifreeze proteins (AFPs) are found in a variety of cold-adapted organisms including fish, insects, plants, bacteria and fungi and promote survival at subzero temperatures by binding to ice crystals and decreasing the freezing temperature of body fluids (Davies et al. 2002; Ewart et al. 1999; Fletcher et al. 2001; Jia and Davies 2002; Yeh and Feeney 1996). Fish AFPs comprise several structurally diverse classes of proteins and are grouped into four types on the basis of their structures: type I AFPs are alanine-rich α-helical proteins (Harding et al. 1999); type II AFPs are cysteine-rich globular proteins containing five disulfide bonds (Liu et al. 2007); type III AFPs are ~7-kDa globular proteins (Jia et al. 1996); and type IV AFPs are glutamate- and glutamine-rich α-helical proteins (Gauthier et al. 2008).

One of most widely studied classes of AFPs is the type III from arctic fish such as the ocean pout (*Zoarces americanus*) and Japanese notched-fin eel pout (*Zoarces elongates* Kner). The type III AFPs have been categorized into two subgroups, quaternary-amino-ethyl (QAE) and sulfopropyl (SP) Sephadex-binding, based on differences in their isoelectric points (Fig. 1a) (Hew et al. 1988). The QAE proteins can be further divided into two subgroups, QAE1 and QAE2 (Fig. 1a) (Nishimiya et al. 2005). Among them, only the QAE1 isoforms exhibit full thermal hysteresis (TH) activities, whereas the others have extremely low or no such activities (Nishimiya et al. 2005). The HPLC12 isoform from the ocean pout, *Z. americanus*, which belongs to the QAE1 subgroup, has been extensively studied by NMR (Chao et al. 1994; Sönnichsen et al. 1996), X-ray crystallography (Jia et al. 1996), mutagenesis (Chao et al. 1994; DeLuca et al. 1998; Graether et al. 1999; Jia et al. 1996), and molecular dynamics (Antson et al. 2001; Chen and Jia 1999). The X-ray structure of the HPLC12 isoform contains one α-helix (residues 37–40), three 3_{10}-helices (residues 19–21, 33–36, and 57–59), and two β-strands (residues 4–7 and 22–25) (Fig. 1a) (Jia et al. 1996). The ice-binding surface (IBS) is comprising residues Q9, P12, N14, T15, A16, T18, V20, M21 and Q44 (Jia et al. 1996) and the flatness of IBS is thought to be important for antifreeze activity (Yang et al. 1998). The molecular dynamics study reported that five additional residues, I13, L19, V41, S42, and K61 are also potentially able to interact with ice (Chen and Jia 1999). Among them, five hydrophilic residues (Q9, N14, T15, T18, and Q44) have the potential to form hydrogen bonds (H-bonds) with water molecule in the ice crystal (Fig. 1b) (Sönnichsen et al. 1996; Jia et al. 1996). The residues, L10, I13, L19, V20, and V41 contributed to ice-binding via hydrophobic interaction with ice and thus replacement by alanine caused significant loss of antifreeze activity (Baardsnes and Davies 2002). Recently, it was reported that the IBS consists of two adjacent surfaces that are flat and relatively hydrophobic (see Fig. 1b) (Garnham et al. 2012). The QAE1 isoform binds both pyramidal and primary prism planes of ice crystal and is able to halt the growth of ice, whereas the SP and QAE2 isoforms exhibit low or no TH activities by binding to only pyramidal ice plane (Garnham et al. 2012). The inactive QAE2 isoform could be converted into a fully-active QAE1-like isoform that is able to bind primary prism ice plane by changing four residues (V9Q/V19L/G20V/I41V) (Garnham et al. 2012).

Sialic acids (*N*-acetylneuraminic acids) play a vital role in a variety of biological functions, such as transmembrane signaling, cell growth, and cell adhesion (Schauer 2004). Sialic acids are synthesized by a conserved enzymatic pathway that includes sialic acid synthase (SAS). Bacterial SAS converts phosphoenolpyruvate (PEP) and N-acetylmannosamine (ManNAc) into *N*-acetylneuraminic acid (NeuNAc, or sialic acid) (Masson and Holbein 1983). Mammalian SAS catalyzes the condensation of PEP and ManNAc 6-phosphate (ManNAc-6P) into NeuNAc 9-phosphate (NeuNAc-9P) which is dephosphorylated into sialic acid (Lawrence et al. 2000). Both enzymes consist of two distinct domains, an N-terminal catalytic NeuB domain (~250 amino acid residues) and a C-terminal antifreeze-like (AFL) domain (~75 amino acid residues). The crystal structure of an SAS from *Neisseria meningitides*, in complex with Mn^{2+}, PEP, and ManNAc, revealed a unique domain-swapped homodimer consisting of an N-terminal $(\alpha/\beta)_8$ barrel-type fold and a C-terminal AFL domain with high structural similarity to the type III AFPs (Gunawan et al. 2005). The AFL domain of the *N. meningitides* SAS (nmAFL) contributed to the substrate binding of the NeuB domain of the opposite monomer via hydrogen bonding (H-bonding) interaction between the side chain of R314 (see Fig. 1a) and the acetyl oxygen of ManNAc (Gunawan et al. 2005). It was proposed that the deletion of the AFL domain in human SAS (hAFL) would abolish the SAS activity, indicating that the hAFL domain might play an important role in substrate binding by the SAS (Hamada et al. 2006). An NMR study of the hAFL domain found that the structure was similar to those of the type III AFPs (Hamada et al. 2006).

Despite having very similar structures, the type III AFP and AFL have very different temperature dependencies of stability and activity. The type III AFP is considered as psychrophilic protein because of the lower working temperature (around 0 °C) while AFL is thought to be mesophilic protein with the working temperature in the range of 20–37 °C. Comparative molecular dynamics studies have been used to elucidate temperature dependence of the dynamics of psychrophilic and mesophilic proteins (Brandsdal et al. 1999; Olufsen et al. 2007; Papaleo et al. 2006, 2007, 2008). A recent molecular dynamics

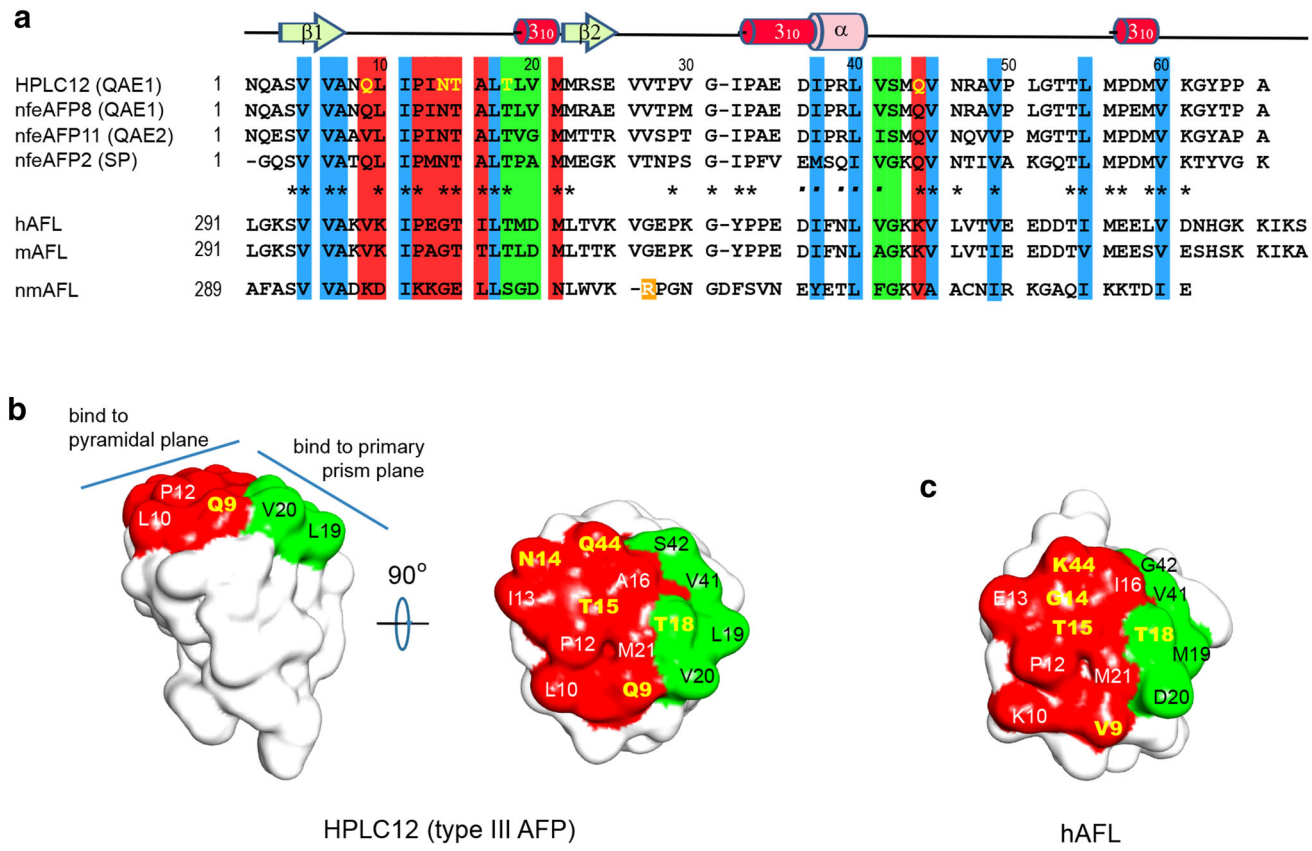

Fig. 1 **a** Multiple sequence alignment of the type III AFP family and AFL domains. NfeAFP2, nfeAFP8, and nfeAFP11 are the isoforms 2, 8, and 11 of the Notched-fin eelpout type III AFP, respectively. hAFL, mAFL, and nmAFL are the AFL domains of human, mouse, and *Neisseria meningitides* SAS, respectively. Numbering and secondary structure elements for HPLC12 are shown above the sequence. *Red* and *green bars* indicate residues composing the pyramidal and primary prism ice plane segments of the IBS, respectively. Five residues (Q9, N14, T15, T18, and Q44) that can form H-bonds with ice crystals are highlighted in *yellow letters*. The *asterisk* and *dot symbols* represent invariant or nearly invariant residues in the type III AFP family, respectively. *Blue bars* indicate the hydrophobic residues that are invariant or nearly invariant residues in the type III AFP family. Substrate-binding R314 in *Neisseria meningitides* SAS is highlighted in *orange*. **b** Two IBS of HPLC12 and **c** the corresponding surfaces of hAFL. Coordinates were derived from the HPLC12 X-ray crystal structure (PDB id = 1MSI) (Jia et al. 1996) and hAFL NMR structure (PDB id = 1WVO) (Hamada et al. 2006). The pyramidal and primary prism ice plane segments of the IBS in the HPLC12 isoform and the corresponding segments in hAFL are shown in *red* and *green*, respectively

simulation study suggested that the type III AFP showed increased overall flexibility at higher temperature compared to the AFL protein (Kundu and Roy 2009). However, the molecular basis of their distinctive behaviors is not well understood.

Heteronuclear NMR spectroscopy is a suitable experimental tool to compare the thermostability and structural flexibility of homologous psychrophilic and mesophilic proteins. In this study, we have investigated backbone dynamics of the type III AFP from ocean pout, *Z. americanus* (HPLC12 isoform) and the AFL domain of human SAS (hAFL) at various temperatures. We also characterized the structural/dynamic properties of the IBS of the HPLC12 and hAFL proteins by analyzing the temperature gradient of the amide proton chemical shift and its correlation with chemical shift deviation (CSD) from random coil. Our results show that the two proteins have entirely different backbone dynamics, especially at low temperature (5 °C). HPLC12 exhibits mostly rigid at low temperature and this rigidity of IBS might be crucial for efficient hydrophobic and H-bonding interaction with ice crystal. Interestingly, most residues of hAFL are relatively rigid at higher temperature (25 °C) while the substrate-binding residues experience distinctive flexible backbone dynamics. Based on our study, we suggest that the dynamic properties of each protein give insight into the underlying causes for the different biological working temperatures of HPLC12 and hAFL. It is very likely that each protein maintains a relatively rigid backbone structure overall, but that the functionally important residues exhibit distinctive dynamics for substrate binding (rigid for ice-binding or flexible for sialic acid binding).

Materials and methods

Sample preparation

The DNA coding sequences for the HPLC12 (M1-A66) and hAFL (L291–S359) were purchased from BIONEER Inc. (Korea) and cloned into *E. coli* expression vectors pET20b (Novagen, USA) with a C-terminal histidine-affinity tag (His-tag) and pET28a (Novagen, USA) with an N-terminal His-tag, respectively. To produce uniformly ^{15}N-labeled or ^{13}C, ^{15}N-labeled HPLC12, C41(DE3) cells were grown in M9 minimal medium that contained 1 g/L $^{15}NH_4Cl$ and/or 2 g/L ^{13}C-glucose as the sole nitrogen and carbon sources. Isotopically-labeled hAFL domain was expressed in a similar manner but in BL21(DE3) cells. The expressed proteins were purified by Ni–NTA affinity and followed by Sephacryl S-100 gel filtration chromatography (GE Healthcare, USA) on a GE AKTA Prime Plus. The concentrations of both proteins were measured using a Pierce BCA Protein Assay Kit (Thermo Scientific, USA). For NMR experiments, the purified proteins were concentrated to 1 mM in a 90 % H_2O/10 % D_2O buffer containing 10 mM sodium phosphate (pH 8.0) and 100 mM NaCl.

NMR experiments

All of the ^{1}H, ^{13}C, and ^{15}N NMR experiments were performed on an Agilent DD2 700-MHz spectrometer (GNU) equipped with a cold probe. All three-dimensional (3D) NMR experiments were carried out with 1 mM ^{13}C, ^{15}N-labeled HPLC12 and hAFL proteins at 25 °C. All 2D ^{1}H/^{15}N-HSQC spectra for HPLC12 and hAFL were obtained using 1 mM ^{15}N-labeled protein samples at various temperature. 1D NMR data were processed with either VNMR J (Agilent, USA) or FELIX2004 (FELIX NMR, USA) software, while the 2D and 3D data were processed with NMRPIPE (Delaglio et al. 1995) and analyzed with Sparky (Goddard and Kneller 2003). 2-2-Dimethyl-2-silapentane-5-sulfonate was used as an external reference.

The backbone resonance assignments for HPLC12 and hAFL were obtained from the following 3D experiments: CACB(CO)NH, HNCACB, HNCA, HNCO, and NOESY-^{1}H/^{15}N-HSQC. The ^{1}H/^{15}N-HSQC spectra of the HPLC12 and hAFL were acquired at temperatures of 5–25 °C in 5 °C increments. The $\Delta\delta/\Delta T$ values of the amide protons were determined from linear variation of the NH chemical shifts with temperature. The amide proton CSDs (δ_{obs}–δ_{rc}) at 25 °C were calculated from the observed chemical shifts (δ_{obs}) and the corresponding random coil (δ_{rc}) values taken from the literature (Andersen et al. 1997).

Backbone dynamics parameters, longitudinal R_1 relaxation rates, transverse R_2 relaxation rates, and $\{^{1}H\}$-^{15}N heteronuclear NOEs were measured using ^{15}N-labeled HPLC12 and hAFL protein samples at 5, 15, and 25 °C. 2D ^{1}H/^{15}N-HSQC spectra for backbone dynamics measurements were acquired with 2,048 (H_N) × 64 (N) data points and 8 scans. Spectral widths of 7,716 Hz (11 ppm) and 2,414 Hz (34 ppm) were used in the H_N and N dimensions, respectively. R_1 values were measured in a series of spectra with relaxation delays of 50, 100, 150, 200, 250, 300, 350, 400, 500, and 600 ms. R_2 measurements were taken with relaxation delays of 10, 30, 50, 70, 90, 110, 130, 150, 190, and 230 ms. For evaluation of $\{^{1}H\}$-^{15}N heteronuclear NOE values, four different data sets with and without an initial proton saturation (2.5 s period) were measured. Reduced spectral density analysis was performed using the following relationships as described by Bracken et al. (1999):

$$\sigma_{NH} = R_1(NOE - 1)\gamma_N/\gamma_H \quad (1)$$

$$J(0.87\omega_H) = 4\sigma_{NH}/(5d^2) \quad (2)$$

$$J(\omega_N) = (4R_1 - 5\sigma_{NH})/(3d^2 + 4c^2) \quad (3)$$

$$J_e(0) = (6R_2 - 3R_1 - 2.72\sigma_{NH})/(3d^2 + 4c^2) \quad (4)$$

where $d = (\mu_o h\gamma_N\gamma_H/8\pi^2)(r_{NH}^{-3})$ and $c = \omega_N\Delta\sigma/\sqrt{3}$, μ_o is the permeability of free space, h is Planck's constant, γ_H and γ_N are the gyromagnetic ratios of the ^{1}H and ^{15}N nuclei, respectively, ω_H and ω_N are the Lamor frequencies, r_{NH} is the average ^{1}H–^{15}N bond length (1.02 Å), and $\Delta\sigma$ is the ^{15}N chemical shift anisotropy (−160 ppm). The effective $J(0)$ [$J_e(0)$] contains contributions from the chemical exchange term, if present.

For well-ordered sites in a macromolecule, the correlation time of overall tumbling motion (τ_m) is obtained from the spectral density functions as (Bracken et al. 1999):

$$\tau_m = \frac{\sqrt{\{J(0) - J(\omega_N)\}/J(\omega_N)}}{\omega_N}. \quad (5)$$

Results and discussion

NMR resonance assignments

The ^{1}H/^{15}N HSQC spectra of the HPLC12 isoform and hAFL domain at 25 °C are shown in Supplementary Fig. S1. Amide backbone resonance assignments for the HPLC12 were made by heteronuclear three-dimensional (3D) NMR experiments at pH 8.0. In hAFL, some amide cross-peaks were missing at pH 8.0, so backbone resonance assignments were conducted at pH 6.0 (see Supplementary Fig. S2). Resonance assignments of hAFL at pH 8.0 were made by comparing of ^{1}H/^{15}N-HSQC spectra acquired at pH 6.0, 6.5, 7.0, and 8.0 and were confirmed by 3D NOESY-^{1}H/^{15}N-HSQC and TOCSY-^{1}H/^{15}N-HSQC spectra at pH 8.0.

Temperature dependence of $^{1}H/^{15}N$-HSQC spectra of HPLC12 and hAFL

The NMR chemical shift is sensitive to the environment of the observed nuclei as well as to temperature-related structural or dynamic changes (Hong et al. 2010; Ohnishi and Urry 1969). As the temperature was lowered, significant cross peak movements were observed in the $^{1}H/^{15}N$ HSQC spectra of the HPLC12 and hAFL proteins (Supplementary Fig. S3). Figure 2 shows the temperature gradients of amide proton chemical shifts ($\Delta\delta/\Delta T$) as a function of residue number (in hAFL, the residue number is starting with residue L291 of SAS as residue L1). In both proteins, most residues have $\Delta\delta/\Delta T$ values >-4.6 ppb/K, indicating that these amides are H-bonded (Cierpicki and Otlewski 2001; Cierpicki et al. 2002). Residues with $\Delta\delta/\Delta T$ values <-4.6 ppb/K (Fig. 2b, c) are in good agreement with the X-ray crystal structure of HPLC12 (Jia et al. 1996) or the NMR structure of hAFL (Hamada et al. 2006), where these amide protons were not protected from exchange by H-bonding.

Residues N14, T15, I37, and V45 in HPLC12 have $\Delta\delta/\Delta T$ values >0 ppb/K. Similarly, in hAFL, the corresponding residues G14, I37, and V45 exhibit positive $\Delta\delta/\Delta T$ values. Residues D20, G27, G42, and E50 in hAFL also have $\Delta\delta/\Delta T$ values >0 ppb/K. The most surprising feature is that some residues (V5, D20, N39, and N62) in hAFL have significantly different $\Delta\delta/\Delta T$ values compared to the corresponding residues in HPLC12 (Fig. 2a). For example, the $\Delta\delta/\Delta T$ value of D20 in hAFL is 0.8 ppb/K, but the corresponding residue V20 in HPLC12 has a $\Delta\delta/\Delta T$ value of −4.7 ppb/K. Instead, the neighboring M19 amide proton exhibits a large negative $\Delta\delta/\Delta T$ (−6.1 ppb/K).

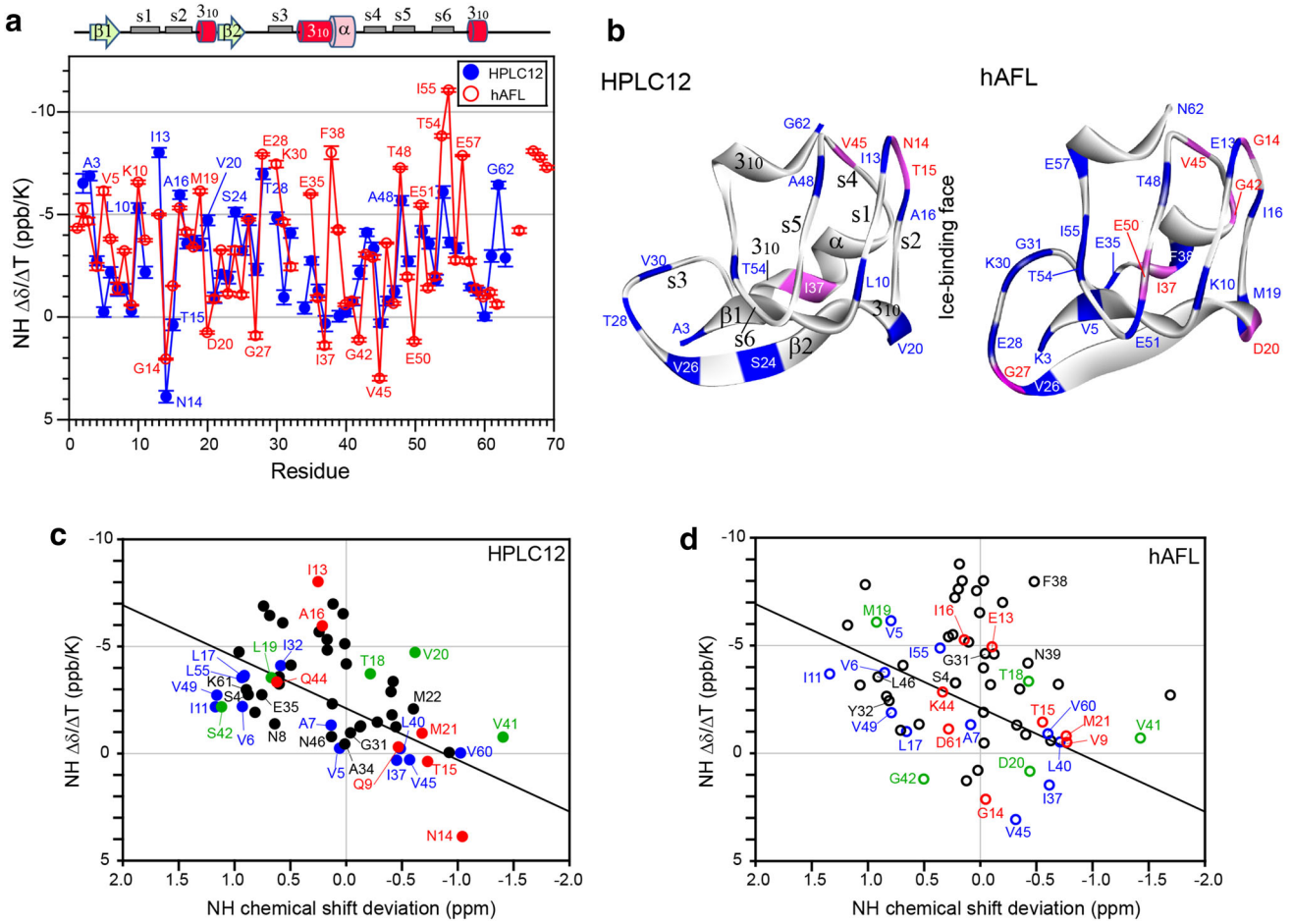

Fig. 2 **a** Temperature dependence of the chemical shifts ($\Delta\delta/\Delta T$) of HPLC12 (*closed blue circles*) and hAFL (*open red circles*) as a function of residue number. Secondary structure models for previously determined **b** X-ray crystal structure of HPLC12 (PDB id = 1MSI) (Jia et al. 1996) and **c** NMR structure of hAFL (PDB id = 1WVO) (Hamada et al. 2006). Residues with $\Delta\delta/\Delta T$ values <-4.6 ppb/K are *colored blue* and residues with $\Delta\delta/\Delta T$ values >0 ppb/K are in *magenta*. The amide proton $\Delta\delta/\Delta T$–CSD correlation plots of **c** HPLC12 and **d** hAFL. *Solid lines* indicate the statistical cutoff, $\Delta\delta/\Delta T = -2.41 \times \text{CSD} - 2.11$. The residues composing the pyramidal and primary prism ice plane segments of the IBS in the HPLC12 isoform and the corresponding segments in hAFL are shown in *red* and *green*, respectively. The hydrophobic residues that are nearly invariant in the type III AFP family are highlighted in *blue*

To characterize in detail the structural and dynamic properties of the HPLC12 and hAFL proteins, a combined analysis of Δδ/ΔT values with CSD (Andersen et al. 1997) was performed. Correlation plots of Δδ/ΔT versus CSD are shown in Figs. 2c, d. The hydrophobic residues, except I32 and V60, that nearly invariant in the type III AFP family were all below the statistical correlation line between Δδ/ΔT and CSD ($\Delta\delta/\Delta T = -2.41 \times CSD - 2.11$) (blue in Fig. 2c), suggesting that these residues are H-bonded and in slow-exchange (Andersen et al. 1997). Similar results were also observed in hAFL with the exception of V5, I55, and V60 (Fig. 2d).

In HPLC12, residues I11 and V49 have Δδ/ΔT values significantly lower than the statistical cutoff (Fig. 2c), reflecting strong H-bonding interactions between the s1 and s5 strands [the strands s1–s6 were random coil in HPLC12 but were assigned as β strands in the type III AFP variant, RD3, from *Rhigophila dearborni* (Miura et al. 2001)] (Supplementary Fig. S4). Similarly, residues N14 and V45 contributed to strong H-bonding interactions between the s2 and s4 strands via N14-NH↔V45-CO and V45-NH↔T15-CO. In addition, four residues in the β1 strand (S4, V5, V6, and A7) and three residues in the second 3_{10} helix (A34, E35, and I37) had Δδ/ΔT that deviated significantly from random coil values (Fig. 2c, Supplementary Fig. S4). In hAFL, significant deviations of Δδ/ΔT values from the statistical cutoff were observed for I11, V49, G14, and V45 (Fig. 2d). However, residues S4 and V5 in the β1 strand and three residues in the α-helix (residues 38, 39 and 41) have significantly higher Δδ/ΔT values compared to the statistical cutoff (Fig. 2d, Supplementary Fig. S4), suggesting that these residues are not strongly H-bonded but are in fast-exchange.

^{15}N NMR relaxation dynamics of HPLC12 at various temperatures

The longitudinal R_1 relaxation rates, transverse R_2 relaxation rates, and {^{1}H}-^{15}N heteronuclear NOEs for uniformly ^{15}N-labeled HPLC12 were measured at three different temperatures (5, 15 and 25 °C) to gain insight into the temperature-dependent dynamic motions of these two proteins (see Figs. 3, 4, 5). R_1 values of HPLC12 are fairly uniform throughout the proteins and increase with temperature (Fig. 3a; Table 1). The R_2 values of HPLC12 are also mostly uniform, with a few exceptions. For example, R_2 of T53 (25.39 Hz) and M59 (19.66 Hz) showed large deviation from the average value at 5 °C (Fig. 3c). The R_2/R_1 ratio was significantly larger than the average value, which implies conformational exchange on the μs–ms timescale (Hong et al. 2010; Tjandra et al. 1995). Interestingly, residues I32, Q44, T53, and M59 exhibited R_2/R_1 ratios above the upper cutoff line [upper/lower cutoff = average ± 1.5 × standard deviation (SD)] at 5 °C, whereas at 25 °C the R_2/R_1 ratios of these residues were below the upper cutoff line (Fig. 4a).

With the exception of the termini, the {^{1}H}-^{15}N heteronuclear NOEs of HPLC12 were mostly >0.8 at all three temperatures, except for V27 at 5 °C (Fig. 5a). This indicates that there are no ps–ns timescale motion in the temperature range studied here.

^{15}N NMR relaxation dynamics of hAFL at various temperatures

The R_1 values of hAFL showed temperature dependence similar to those of HPLC12 (Fig. 3b). Residues G27–G31 and E35 showed slightly elevated R_1 values compared to other residues except both termini at all three temperatures (Fig. 3b). The R_2 values increased and showed larger deviation from the average values as the temperature decreased (Fig. 3d; Table 1). Residues K30, G31, and I37 exhibited significantly larger R_2/R_1 ratios than the average at 25 °C (Fig. 4b). Line broadening prevented the R_2/R_1 ratios for E28, K30, and G31 at 5 °C from being determined (Supplementary Fig. S3). At 5 °C, three more residues (K25, E58, and V60) show larger R_2/R_1 ratios than the upper cutoff value (Fig. 4b). Residues K3, G27, and D51 have significantly smaller R_2/R_1 ratios than the average value at 5 °C (Fig. 4b).

The {^{1}H}-^{15}N heteronuclear NOEs of hAFL exhibit very different patterns from those of HPLC12 (Figs. 4, 5). Several residues had NOE values ≤0.8 and this number increased when the temperature dropped (Fig. 5d). At 25 °C, some residues (K3, K10, V24, V26–G31, K44, E50, I55–E57 and N62) had NOE values ≤0.8. The NOE values for residues K3, K30, and G31 could not be determined due to line broadening at 5 °C. Residues S4, E13, I16, D20, V26–G31, L40–G42, K44, V45, T48–E50, D53, T54, and E57–N62 had NOEs ≤0.8 or showed very weak resonances at 5 °C (Fig. 5d). It is noteworthy that the structural flexibility of hAFL on the ps–ns timescale increased as the temperature decreased, in contrast to HPLC12. Interestingly, residues K10 and K44 that showed NOEs <0.8 are located on the corresponding surfaces of ice-binding site even at 25 °C (Fig. 5d). Residues G7, V24, V26, G27, E28, K30 and G31 that showed NOEs <0.8 at 25 °C (Fig. 5d) are clustered on the substrate-binding surface for bacterial SAS (Hamada et al. 2006). Residue K44 of hAFL showed NOE values ≤0.8 at all three temperatures, while the corresponding Q44 of HPLC12 had NOE values >0.8 through all temperatures. As mentioned above, Q44 of HPLC12 may experience conformational exchange on the μs–ms timescale at low temperature. Taken together, our data indicate that the IBS of HPLC12 and the corresponding surface of hAFL have different dynamic properties at low temperature.

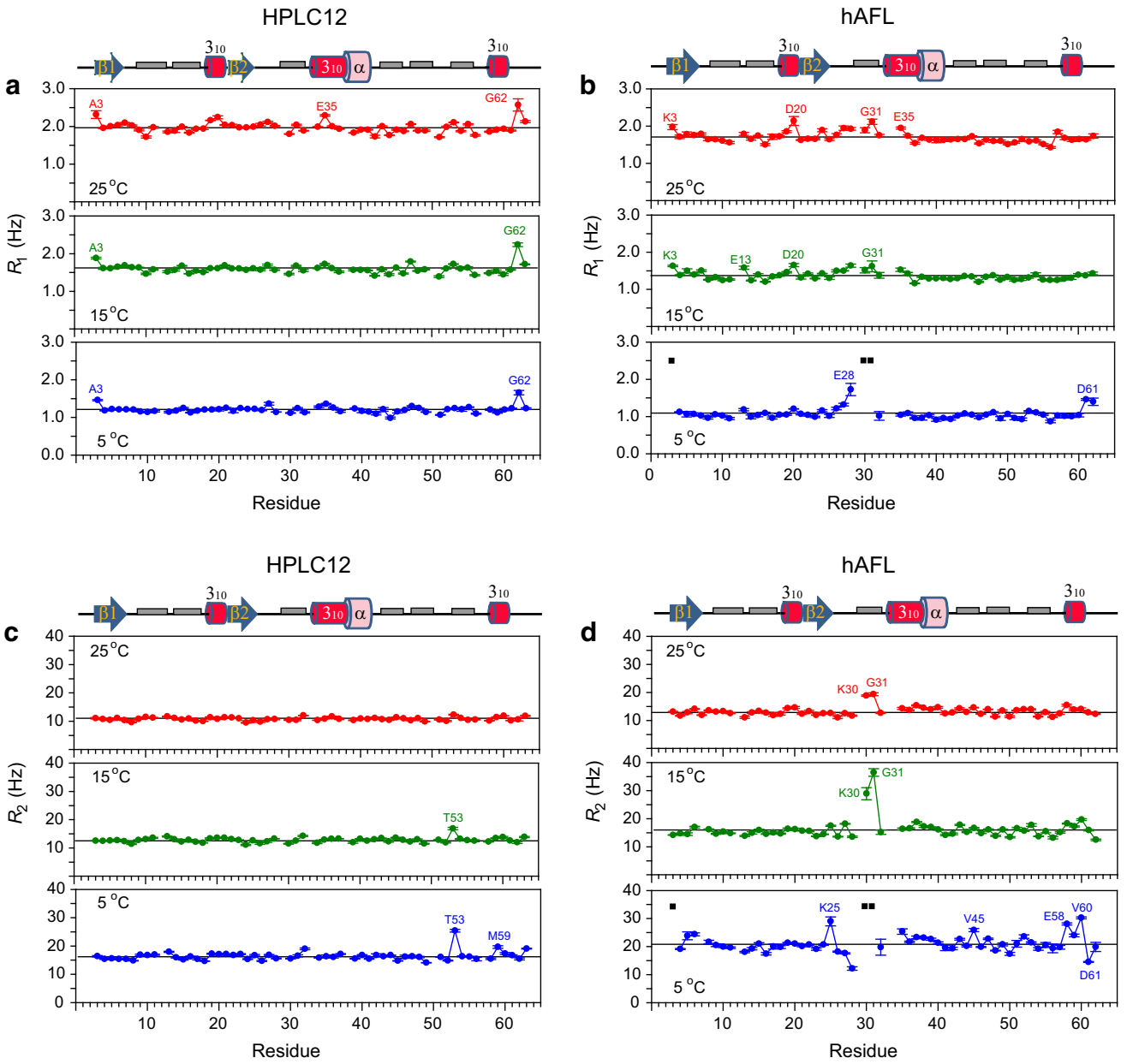

Fig. 3 ^{15}N relaxation parameters of HPLC12 and hAFL as a function of residue number. R_1 relaxation rates of **a** HPLC12 and **b** hAFL are determined at 5 °C (*lower*, *blue*), 15 °C (*middle*, *green*), and 25 °C (*upper*, *red*). R_2 relaxation rates of **c** HPLC12 and **d** hAFL are determined at 5 °C (*lower*, *blue*), 15 °C (*middle*, *green*), and 25 °C (*upper*, *red*). The *error bars* represent curve fitting errors during the determination of R_1 and R_2 values from experiment data. The *solid lines* indicate the average values. In hAFL, the R_1 and R_2 relaxation rates of A7 at 5 and 15 °C could not be determined because of overlapping with other resonance. The *black square symbols* indicate residues whose relaxation data could not be determined because of severe line-broadening at 5 °C

Analysis of ^{15}N NMR relaxation parameters in terms of reduced spectral density

The ^{15}N-relaxation data at three different temperatures were used to calculate reduced spectral density function J-values. Figure 6 shows $J_e(0)$, $J(\omega_N)$, and $J(0.87\omega_H)$ of HPLC12 and hAFL determined at three temperatures. The temperature dependence of $J_e(0)$ was similar to R_2, and that of $J(\omega_N)$ was similar to the R_1 pattern. HPLC12 had fairly uniform $J_e(0)$ values with the average values of 4.24 ns/rad at 5 °C, 3.22 ns/rad at 15 °C, and 2.63 ns/rad at 25 °C (Table 1). Residues I32 (4.94 ns/rad), T53 (6.64 ns/rad), M59 (5.12 ns/rad), and Y63 (4.94 ns/rad) had significantly larger $J_e(0)$ values than the average at

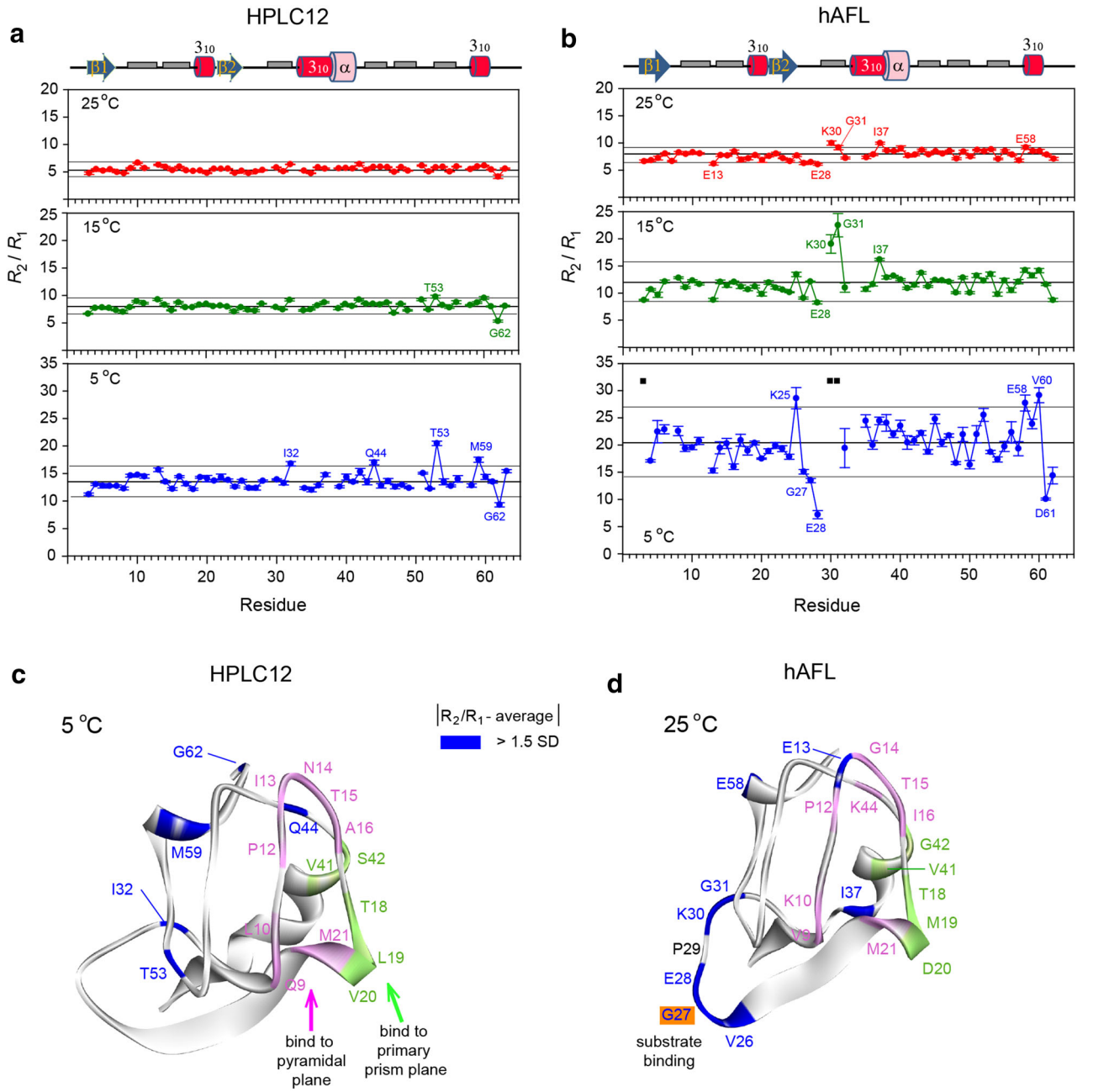

Fig. 4 R_2/R_1 ratios of **a** HPLC12 and **b** hAFL as a function of residue number are determined at 5 (*lower*, *blue*), 15 (*middle*, *green*), and 25 °C (*upper*, *red*). The *error bars* represent the standard deviations of R_2/R_1 ratios ($\sigma_{R2/R1}$) determined by using equation, $\sigma_{R2/R1} = R_2/R_1\sqrt{(\sigma_{R2}/R_2)^2 + (\sigma_{R2}/R_2)^2}$, where σ_{R1} and σ_{R2} are curve fitting errors during the determination of R_1 and R_2 values, respectively. The *thick* and *two thin solid lines* indicate the average and upper/lower cutoff values (average ± 1.5 × SD), respectively. The *black square symbols* indicate residues whose relaxation data could not be determined because of severe line-broadening at 5 °C. Mapping of the R_2/R_1 ratios onto the secondary structure models of **c** HPLC12 and **d** hAFL. Residues which have deviated R_2/R_1 ratios than the upper/lower cutoff lines are shown in *blue*. Residues composing the pyramidal and primary prism ice plane segments of HPLC12 and corresponding residues of hAFL are shown in *pink* and *light green*, respectively. Residue G27 of hAFL, which is corresponding the substrate-binding R27 in *Neisseria meningitides* SAS, is in *orange*

5 °C (Fig. 6a). This indicates that these residues are involved in μs–ms timescale motions (Lefevre et al. 1996). $J(\omega_N)$ and $J(0.87\omega_H)$ of HPLC12 were also mostly uniform (Fig. 6a). The small $J(0.87\omega_H)$ values imply that HPLC12 is well structured with limited internal mobility at all three temperatures, which is consistent with the uniformly high $\{^1H\}$-^{15}N heteronuclear NOE values.

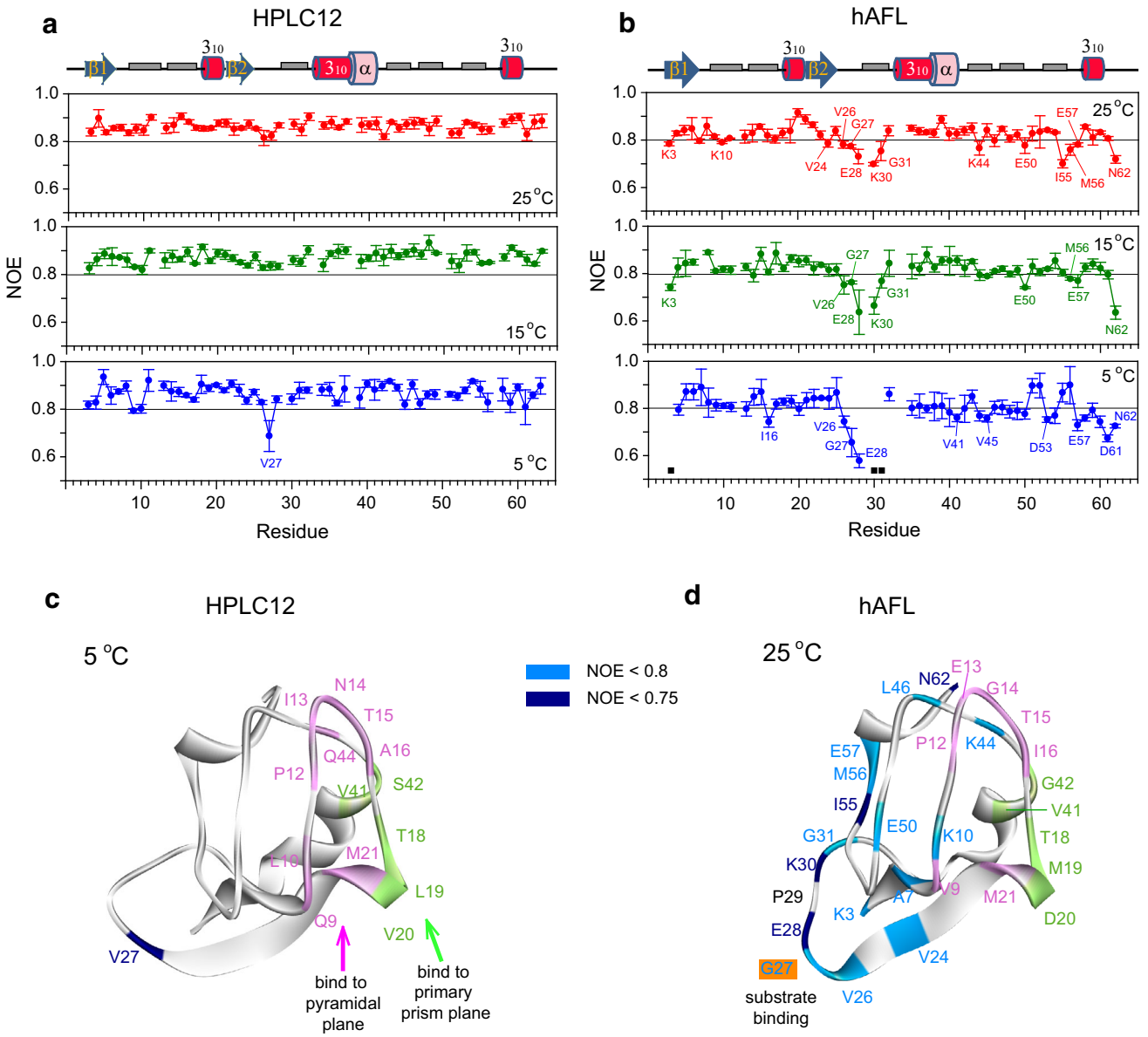

Fig. 5 Heteronuclear $\{^1H\}$-^{15}N NOEs of **a** HPLC12 and **b** hAFL as a function of residue number are determined at 5 °C (*lower*, *blue*), 15 °C (*middle*, *green*), and 25 °C (*upper*, *red*). The *error bars* of the heteronuclear NOE data represent standard deviations of four different data sets. In hAFL, the heteronuclear NOE of A7 at 5 and 15 °C could not be determined because of overlapping with other resonance. The *black square symbols* indicate residues whose relaxation data could not be determined because of severe line-broadening at 5 °C. Mapping of the $\{^1H\}$-^{15}N NOEs onto the secondary structure models of **c** HPLC12 and **d** hAFL. Residues which have smaller heteronuclear NOE <0.8 or <0.75 are shown in *light blue* and *dark blue*, respectively. Residues composing the pyramidal and primary prism ice plane segments of HPLC12 and corresponding residues of hAFL are shown in *pink* and *light green*, respectively. Residue G27 of hAFL, which is corresponding the substrate-binding R27 in *Neisseria meningitides* SAS, is in *orange*

In contrast, hAFL showed higher and more varied $J_e(0)$ because of more deviation in R_2. The average $J_e(0)$ values were 5.48 ns/rad at 5 °C, 4.16 ns/rad at 15 °C, and 3.33 ns/rad at 25 °C (Table 1). The elevated average $J_e(0)$ values of hAFL imply that there are more residues that experience slow motions. Residues K25, E58, and V60 which showed larger R_2/R_1 ratios as well as significantly higher $J_e(0)$ values than the average at 5 °C (Figs. 4b, 6b). As mentioned previously, abnormally large values of $J_e(0)$ indicate that these residues are experiencing μs–ms time-scale motions. At all three temperatures, the $J(0.87\omega_H)$ values of hAFL are much larger and show more deviation than those HPLC12, implying that the hAFL domain exhibits greater ps–ns internal motion compared to HPLC12.

The correlation times of overall tumbling motion (τ_m) of HPLC12 and hAFL are obtained from the spectral density functions as using Eq. 4 (Supplementary Fig. S5). The residues that have R_2/R_1 ratio deviated from upper/lower

Table 1 The average ^{15}N relaxation parameters of HPLC12 and hAFL determined at 5, 15, and 25 °C

	HPLC12[a]			hAFL[b]		
	5 °C	15 °C	25 °C	5 °C	15 °C	25 °C
R_1 (Hz)	1.21 ± 0.10	1.60 ± 0.13	1.97 ± 0.15	1.07 ± 0.15	1.37 ± 0.12	1.70 ± 0.15
R_2 (Hz)	16.41 ± 1.64	12.81 ± 0.90	10.80 ± 0.61	20.96 ± 3.17	15.85 ± 2.38	13.26 ± 1.57
R_2/R_1	13.66 ± 1.69	8.06 ± 0.79	5.50 ± 0.50	20.10 ± 4.13	11.71 ± 1.87	7.81 ± 0.89
$J_e(0)$ (ns/rad)	4.24 ± 0.44	3.22 ± 0.24	2.63 ± 0.16	5.48 ± 0.86	4.16 ± 0.97	3.33 ± 0.42
$J(\omega_N)$ (ns/rad)	0.21 ± 0.02	0.28 ± 0.02	0.35 ± 0.03	0.19 ± 0.02	0.24 ± 0.02	0.30 ± 0.03
$J(0.87\omega_H)$ (ps/rad)	2.56 ± 0.87	3.23 ± 0.74	4.17 ± 0.72	3.43 ± 1.63	4.05 ± 1.38	4.91 ± 1.30
τ_m (ns)[c]	9.74 ± 0.42	7.30 ± 0.32	5.78 ± 0.31	12.16 ± 0.95	9.02 ± 0.53	7.15 ± 0.36

[a] The average values of residues 3–63

[b] The average values of residues 3–62

[c] Residues that exhibit an R_2/R_1 ratio deviated from upper/lower cutoff values or have an NOE <0.7 are excluded from calculation of the average τ_m values

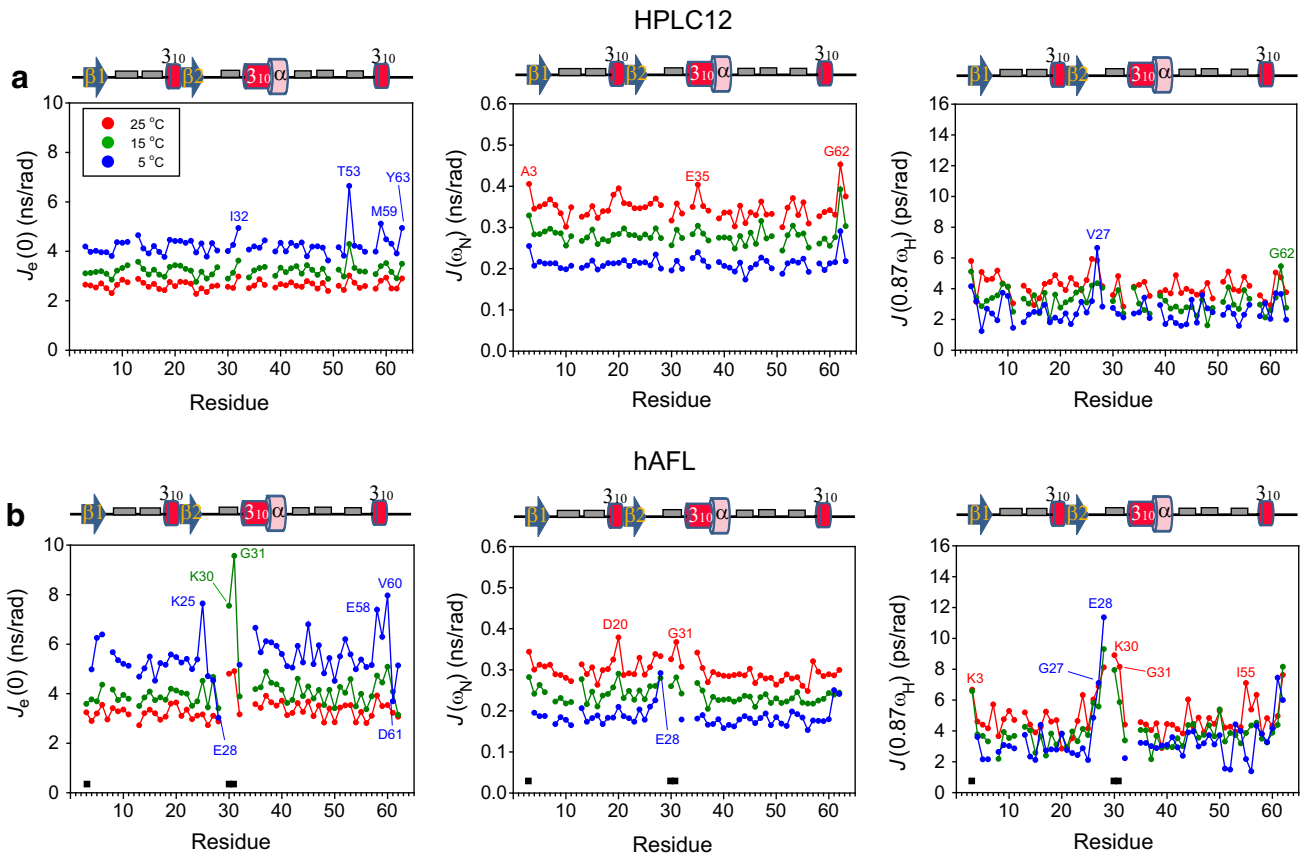

Fig. 6 Reduced spectral density functions of HPLC12 and hAFL. $J_e(0)$ (*left*); $J(\omega_N)$ (*middle*); and $J(0.87\omega_H)$ (*right*) are calculated for **a** HPLC12 and **b** hAFL as a function of residue number determined at 5 °C (*lower*, *blue*), 15 °C (*middle*, *green*), and 25 °C (*upper*, *red*)

cutoff values or heteronuclear NOE <0.7 are excluded from calculation of the average τ_m values. We determined that the average τ_m values of HPLC12 were 9.74 ns at 5 °C, 7.30 ns at 15 °C, and 5.78 ns at 25 °C (Table 1). Similarly, hAFL have the average τ_m values of 12.16 ns at 5 °C, 9.02 ns at 15 °C, and 7.15 ns at 25 °C (Table 1). If HPLC12 and hAFL are monomeric, we would expect the average τ_m values of approximately 8.1 ns for HPLC12 (8.1 kDa with C-terminal His-tag) and 9.9 ns for hAFL (9.9 kDa with N-terminal His-tag) at 5 °C by using

relation, $\tau_m \sim$ Mw, at 5 °C (Graether et al. 2003). Our experimental τ_m values for both proteins are slightly larger than what would be predicted from their molecular weights.

Functional implications of HPLC12 and hAFL

In this study, ^{15}N NMR relaxation experiments in the temperature range of 5–25 °C were used to characterize the unique backbone dynamics of the psychrophilic protein, HPLC12 and compare them to those of a homologous mesophilic protein hAFL. HPLC12 had fairly uniform R_1 and R_2 values at all three temperatures, whereas the R_2 values of hAFL showed much larger deviations from the average values as the temperature decreased (Fig. 3). This means that HPLC12 has a more rigid backbone structure and lacks conformational exchange on the μs–ms timescale for most residues even at low temperature. This result is consistent with previous reports that the insect β-helical AFPs from *Tenebrio molitor* and spruce budworm are well structured and become more rigid as the temperature is lowered (Daley et al. 2002; Graether et al. 2003). This study also found that the mesophilic protein, hAFL, shows significant flexibility and exchange in backbone dynamics at 5 °C compared to the psychrophilic protein, HPLC12. This is evident from: i) large deviations in R_2 values (μs–ms timescale motion) and ii) $\{^1H\}$-^{15}N heteronuclear NOEs $\leq$0.8 (ps–ns timescale motion) (Figs. 3, 5). These results indicate that the backbone of hAFL displays significant conformational exchange at low temperature, even though the protein is ordered at 25 °C.

With the exception of the termini, most residues of HPLC12 had $\{^1H\}$-^{15}N heteronuclear NOEs >0.8, whereas in hAFL, the number of residues displaying $\{^1H\}$-^{15}N heteronuclear NOEs $\leq$0.8 increased as the temperature decreased (Fig. 5). These data indicate that HPLC12 has very little backbone flexibility on the ps–ns timescale over the temperature range of 5–25 °C, which is consistent with its small $J(0.87\omega_H)$ values. These results imply that HPLC12 is well structured and has limited internal mobility at all three temperatures, hAFL, on the other hand, show greater backbone flexibility on the ps–ns timescale with remarkably higher values of $J(0.87\omega_H)$ for several residues at 25 °C, and this structural flexibility increased as the temperature decreased. In addition, hAFL displayed significant slow motions (μs–ms timescale) at the low temperature. Taken together, our data suggest that psychrophilic proteins like HPLC12 exhibit a rigid backbone structure with internal dynamics that remain unaffected by temperature, whereas mesophilic proteins like hAFL have less rigid backbones and specific residues whose conformational mobilities increase significantly at low temperature.

Since the biologically relevant temperature of HPLC12 is subzero, the NMR dynamics data at low temperature may provide insight into the molecular mechanism of its anti freezing activity. We found several unique features of the backbone structure and dynamics of HPLC12 at low temperature from our temperature-dependent NMR dynamics study. First, most of hydrophobic residues which are invariant or nearly invariant in the type III AFP family were below the statistical cutoff line in the correlation plot of $\Delta\delta/\Delta T$ versus CSD (Fig. 2c). These results suggest that the amide protons of these residues are protected from exchange with solvent via H-bonding interactions and they can play important roles in protein folding of the type III AFPs. As shown in Supplementary Fig. S4A, the H-bonding interactions established between the s1 and s5 strands and between the s2 and s4 strands as well as in the β1 sheet and the second 3_{10} helix may contribute energetically to the rigid backbone structure of HPLC12 for efficient ice-binding at low temperature. However, in hAFL, the β1 strand (S4 and V5) and α-helix (F38, N39, and V41) are not H-bonded and show a fast-exchange pattern, which could partially explain why hAFL, especially in the s3 region, displays conformational flexibility at low temperature.

The ice-binding residues of HPLC12 exhibit distinct dynamics features compared to the corresponding residues of hAFL. The structural study of insect β-helical AFPs proposed an "anchored clathrate mechanism" where both the hydrophobic effect and H-bonding contributed to adsorption of AFP to ice (Garnham et al. 2011). Previous NMR relaxation studies of the insect β-helical AFPs revealed that the TXT side-chains on the IBS are highly rigid (Daley et al. 2002; Graether et al. 2003; Graether and Sykes 2004). It was reported that the Thr side-chains on the IBS of the *Tenebrio moliter* AFP adopt a preferred rotameric conformation at low temperature (Daley et al. 2004). The rigidity of the IBS suggests that AFP maintains surface-to-surface complementarity between the AFP and ice crystal, wherein the rigid array of Thr side-chains is capable of forming efficient hydrophobic and H-bonding interactions (Daley et al. 2004). Our backbone dynamics study also showed that all residues on the IBS of HPLC12 are rigid with high heteronuclear NOE values (Fig. 5) as well as little deviations of the R_2/R_1 ratio from the average value (Fig. 4). In the active QAE1-isoform of the type III AFP, the surface pocket created by residues Q9, T18, V20, and M21 traps the ice-like water that anchor the AFP-ice interaction (Kumeta et al. 2013). The hydrogen-deuterium exchange experiments revealed that these four residues in the active QAE1-like isoform are rigid and capable of forming the surface pocket, while the corresponding residues of the inactive QAE2-isoform cannot form the pocket (Kumeta et al. 2013). Taken together, our NMR study

support an "anchored clathrate mechanism" of the type III AFP where the IBS exhibits rigid structure for efficient hydrophobic and H-bonding interaction with ice crystal and is capable of trapping ice-like water into surface pocket that anchor the AFP-ice interaction.

Although HPLC12 has fairly uniform R_1 and R_2 values at all three temperatures, some residues (I32, Q44, T53, and M59) have significantly larger R_2/R_1 ratios than the average value at 5 °C (Fig. 4a). As expected from R_2/R_1 ratios, these residues have significantly larger $J_e(0)$ values than the average at 5 °C (Fig. 6a), which strongly support the slow exchange of these residues on the μs–ms timescale. The internal motion of residue Q44 might be required for efficient H-bonding of its side-chain with the ice crystal. However, residues I32, T53, and M59 are far from the IBS of HPLC12, indicating that the conformational exchange on the μs–ms timescale of these residues at low temperature might not be crucial for interaction with ice crystal.

At 25 °C, the R_1 and R_2 values of the mesophilic protein, hAFL, are uniform throughout and the $\{^1H\}$-^{15}N heteronuclear NOEs >0.8 for most residues, indicating that hAFL displays a rigid backbone structure at ambient temperature. Interestingly, residues located at the loop region (V26–Y32) between the β2 sheet and the second 3_{10} helix show significant flexibility and exchange in backbone dynamics even at 25 °C evident from: i) large deviations in R_1 and R_2 values (μs–ms timescale motion) and ii) $\{^1H\}$-^{15}N heteronuclear NOEs ≤0.8 (ps–ns timescale motion) (Figs. 3, 5). In contrast, the corresponding residues of HPLC12 show no deviated R_2/R_1 ratios (Fig. 4a) as well as heteronuclear NOE >0.8 (Fig. 5a) at 25 °C, indicating this loop region of HPLC12 has rigid backbone structure. In addition, residues I55–E58 also experience flexible internal motion (see Figs. 4b, 5b). Among them, residues V26, E28, and G31 are class-specific residues of the vertebrate AFL domain (Hamada et al. 2006). The crystal structure of an *N. meningitides* SAS found that the highly conserved R314 (highlighted in orange as R27 in Fig. 1a) protrudes to form direct of water-mediated H-bond with ManNAc (Gunawan et al. 2005). The importance of R314 in the catalytic activity of SAS is supported by inhibition study of *Streptococcus agalactiae* SAS through the addition of an arginine directed modifying reagent (Suryanti et al. 2003). In the vertebrate AFL domains, this Arg residue is missing from the ligand-binding site, but some class-specific residues (K8 and K25 in Fig. 1a) with positively charged side-chains lie near the substrate (Hamada et al. 2006). Interestingly, we found flexible regions clustered around the corresponding residue in hAFL, G27 (Figs. 4d, 5d). Thus, it is reasonable to think that the flexibility of these regions may contribute to the biological function of the AFL domain in SAS. In contrast, the IBS of the insect β-helical AFP exhibits rigid backbone structure and the ice-binding Thr residues participate in intrastrand H-bonds that stabilize the flat surface required for optimal ice-binding (Daley et al. 2004). Instead, the Thr side-chains on the IBS are flexible to adopt a preferred ice-binding conformation without an entropic penalty (Daley and Sykes 2003).

Conclusions

In this study, we have compared the dynamic properties of the type III AFP (HPLC12 isoform) and the AFL domain of human SAS (hAFL) by analyzing the temperature gradient of the amide proton chemical shift, its correlation with CSD from random coil, backbone dynamics, and reduced spectral density. Our data show that the two homologous proteins have distinctive backbone dynamics. Most residues of HPLC12 are rigid while a few residues on the IBS experience conformational exchange on the μs–ms timescale at 5 °C. In contrast, hAFL is remarkably flexible at 5 °C, and its flexibility decreases at higher temperatures (25 °C). At the same time, the residues that are involved in substrate binding show fast internal motion. Based on our study, we suggest that the dynamic properties of each protein give insight into the basis for the different physiological working temperatures of HPLC12 and hAFL. It is very likely that each protein maintains a relatively rigid backbone structure overall, but that the functionally important residues exhibit distinctive dynamics for substrate binding (rigid for ice-binding or flexible for sialic acid binding).

Acknowledgments This work was supported by several National Research Foundation of Korea (NRF) Grants funded by the Korean Government (MSIP) [2010-0020480, 2013R1A2A2A05003837, 2012R1A4A1027750 (BRL)]. This work was also supported by a Grant from the Next-Generation BioGreen 21 Program (SSAC, No. PJ009041), Rural Development Administration, Korea. We thank the GNU Central Instrument Facility for performing the NMR experiments and Dr. Melissa Stauffer and Miss Laura Mizoue, of Scientific Editing Solutions, for editing the manuscript.

References

Andersen NH, Neidigh JW, Harris SM et al (1997) Extracting information from the temperature gradients of polypeptide NH chemical shifts. 1. the importance of conformational averaging. J Am Chem Soc 119:8547–8561

Antson AA, Smith DJ, Roper DI et al (2001) Understanding the mechanism of ice binding by type III antifreeze proteins. J Mol Biol 305:875–889

Baardsnes J, Davies PL (2002) Contribution of hydrophobic residues to ice binding by fish type III antifreeze protein. Biochim Biophys Acta 1601:49–54

Bracken C, Carr PA, Cavanagh J, Palmer AG (1999) Temperature dependence of intramolecular dynamics of the basic leucine zipper of GCN4: implications for the entropy of association with DNA. J Mol Biol 285:2133–2146

Brandsdal BO, Heimstad ES, Sylte I, Smalås AO (1999) Comparative molecular dynamics of mesophilic and psychrophilic protein homologues studied by 1.2 ns simulations. J Biomol Struct Dyn 17:493–506

Chao H, Sönnichsen FD, DeLuca CI et al (1994) Structure-function relationship in the globular type III antifreeze protein: identification of a cluster of surface residues required for binding to ice. Protein Sci 3:1760–1769

Chen G, Jia Z (1999) Ice-binding surface of fish type III antifreeze. Biophys J 77:1602–1608

Cierpicki T, Otlewski J (2001) Amide proton temperature coefficients as hydrogen bond indicators in proteins. J Biomol NMR 21: 249–261

Cierpicki T, Zhukov I, Byrd RA, Otlewski J (2002) Hydrogen bonds in human ubiquitin reflected in temperature coefficients of amide protons. J Magn Reson 157:178–180

Daley ME, Sykes BD (2003) The role of side chain conformational flexibility in surface recognition by *Tenebrio molitor* antifreeze protein. Protein Sci 12:1323–1331

Daley ME, Spyracopoulos L, Jia Z et al (2002) Structure and dynamics of a β-helical antifreeze protein. Biochemistry 41: 5515–5525

Daley ME, Graether SP, Sykes BD (2004) Hydrogen bonding on the ice-binding face of a β-helical antifreeze protein indicated by amide proton NMR chemical shifts. Biochemistry 43:13012–13017

Davies PL, Baardsnes J, Kuiper MJ, Walker VK (2002) Structure and function of antifreeze proteins. Philos Trans R Soc Lond B 357: 927–935

Delaglio F, Grzesiek S, Vuister GW et al (1995) NMRPipe: a multidimensional spectral processing system based on UNIX pipes. J Biomol NMR 6:277–293

DeLuca CI, Davies PL, Ye Q, Jia Z (1998) The effects of steric mutations on the structure of type III antifreeze protein and its interaction with ice. J Mol Biol 275:515–525

Ewart KV, Lin Q, Hew CL (1999) Structure, function and evolution of antifreeze proteins. Cell Mol Life Sci 55:271–283

Fletcher GL, Hew CL, Davies PL (2001) Antifreeze proteins of teleost fishes. Annu Rev Physiol 63:359–390

Garnham CP, Campbell RL, Davies PL (2011) Anchored clathrate waters bind antifreeze proteins to ice. Proc Natl Acad Sci USA 108:7363–7367

Garnham CP, Nishimiya Y, Tsuda S et al (2012) Engineering a naturally inactive isoform of type III antifreeze protein into one that can stop the growth of ice. FEBS Lett 586:3876–3881

Gauthier SY, Scotter AJ, Lin FH et al (2008) A re-evaluation of the role of type IV antifreeze protein. Cryobiology 57:292–296

Goddard TD, Kneller DG (2003) SPARKY 3. University of California, San Francisco

Graether SP, Sykes BD (2004) Cold survival in freeze-tolerant insects: structure and function of beta-helica proteins. Eur J Biochem 271:3285–3296

Graether SP, DeLuca CI, Baardsnes J et al (1999) Quantitative and qualitative analysis of type III antifreeze protein structure and function. J Biol Chem 274:11842–11847

Graether SP, Gagné SM, Spyracopoulos L et al (2003) Spruce budworm antifreeze protein: changes in structure and dynamics at low temperature. J Mol Biol 327:1155–1168

Gunawan J, Simard D, Gilbert M et al (2005) Structural and mechanistic analysis of sialic acid synthase NeuB from Neisseria meningitidis in complex with Mn^{2+}, phosphoenolpyruvate, and N-acetylmannosaminitol. J Biol Chem 280:3555–3563

Hamada T, Ito Y, Abe T et al (2006) Solution structure of the antifreeze-like domain of human sialic acid synthase. Protein Sci 15:1010–1016

Harding MM, Ward LG, Haymet AD (1999) Type I 'antifreeze' proteins. Structure-activity studies and mechanisms of ice growth inhibition. Eur J Biochem 264:653–665

Hew CL, Wang NC, Joshi S et al (1988) Multiple genes provide the basis for antifreeze protein diversity and dosage in the ocean pout, *Macrozoarces americanus*. J Biol Chem 263:12049–12055

Hong J, Hu Y, Li C et al (2010) NMR characterizations of the ice binding surface of an antifreeze protein. PLoS One 5:e15682

Jia Z, Davies PL (2002) Antifreeze proteins: an unusual receptor-ligand interaction. Trends Biochem Sci 27:101–106

Jia Z, DeLuca CI, Chao H, Davies PL (1996) Structural basis for the binding of a globular antifreeze protein to ice. Nature 384: 285–288

Kumeta H, Ogura K, Nishimiya Y et al (2013) NMR structure note: a defective isoform and its activity-improved variant of a type III antifreeze protein from *Zoarces elongates* Kner. J Biomol NMR 55:225–230

Kundu S, Roy D (2009) Comparative structural studies of psychrophilic and mesophilic protein homologues by molecular dynamics simulation. J Mol Graph Model 27:871–880

Lawrence SM, Huddleston KA, Pitts LR et al (2000) Cloning and expression of the human *N*-acetylneuraminic acid phosphate synthase gene with 2-keto-3-deoxy-D-glycero-D-galacto-nononic acid biosynthetic ability. J Biol Chem 275:17869–17877

Lefevre JF, Dayie KT, Peng JW, Wagner G (1996) Internal mobility in the partially folded DNA binding and dimerization domains of GAL4: NMR analysis of the N-H spectral density functions. Biochemistry 35:2674–2686

Liu Y, Li Z, Lin Q et al (2007) Structure and evolutionary origin of Ca^{2+}-dependent herring type II antifreeze protein. PLoS One 2: e548

Masson L, Holbein BE (1983) Physiology of sialic acid capsular polysaccharide synthesis in serogroup B Neisseria meningitidis. J Bacteriol 154:728–736

Miura K, Ohgiya S, Hoshino T et al (2001) NMR analysis of type III antifreeze protein intramolecular dimer. Structural basis for enhanced activity. J Biol Chem 276:1304–1310

Nishimiya Y, Sato R, Takamichi M et al (2005) Co-operative effect of the isoforms of type III antifreeze protein expressed in Notched-fin eelpout, *Zoarces elongatus* Kner. FEBS J 272:482–492

Ohnishi M, Urry DW (1969) Temperature dependence of amide proton chemical shifts: the secondary structures of gramicidin S and valinomycin. Biochem Biophys Res Commun 36:194–202

Olufsen M, Brandsdal BO, Smalås AO (2007) Comparative unfolding studies of psychrophilic and mesophilic uracil DNA glycosylase: MD simulations show reduced thermal stability of the cold-adapted enzyme. J Mol Graph Model 26:124–134

Papaleo E, Riccardi L, Villa C et al (2006) Flexibility and enzymatic cold-adaptation: a comparative molecular dynamics investigation of the elastase family. Biochim Biophys Acta 1764:1397–1406

Papaleo E, Olufsen M, De Gioia L, Brandsdal BO (2007) Optimization of electrostatics as a strategy for cold-adaptation: a case study of cold- and warm-active elastases. J Mol Graph Model 26:93–103

Papaleo E, Pasi M, Riccardi L et al (2008) Protein flexibility in psychrophilic and mesophilic trypsins. Evidence of evolutionary conservation of protein dynamics in trypsin-like serine-proteases. FEBS Lett 582:1008–1018

Schauer R (2004) Sialic acids: fascinating sugars in higher animals and man. Zoology 107:49–64

Sönnichsen FD, DeLuca CI, Davies PL, Sykes BD (1996) Refined solution structure of type III antifreeze protein: hydrophobic

groups may be involved in the energetics of the protein–ice interaction. Structure 4:1325–1337

Suryanti V, Nelson A, Berry A (2003) Cloning, over-expression, purification, and characterisation of *N*-acetylneuraminate synthase from *Streptococcus agalactiae*. Protein Expr Purif 27:346–356

Tjandra N, Feller SE, Pastor RW, Bax A (1995) Rotational diffusion anisotropy of human ubiquitin from ^{15}N NMR relaxation. J Am Chem Soc 117:12562–12566

Yang DSC, Hon WC, Bubanko S et al (1998) Identification of the ice-binding surface on a type III antifreeze protein with a "flatness function" algorithm. Biophys J 74:2142–2151

Yeh Y, Feeney RE (1996) Antifreeze proteins: structures and mechanisms of function. Chem Rev 96:601–618